ISSN/2499-5347

**S. GAGLIARDI, M. GHEZELBASH, M. FALCONIERI**

Fusion and Technologies for Nuclear Safety Department
Physical Technologies for Safety and Health Division
Casaccia Research Center, Rome

**M. MARROCCO**

Department of Energy Technologies and Renewable Sources
Division of Production, Storage and Use of Energy
Laboratory of Processes and Systems Engineering for Energy Decarbonization
Casaccia Research Center, Rome

**C. MERLA**

Department of Sustainability of Production and Territorial Systems and Energy Efficiency
Technologies and Methodologies for Health Protection Division
Biomedical Technologies Laboratory
Casaccia Research Center, Rome

**F. RONDINO**

Fusion and Technologies for Nuclear Safety Department
Physical Technologies for Safety and Health Division
Micro and Nanostructures Laboratory for Photonics
Casaccia Research Center, Rome

# DESIGN AND OPERATION OF A FEMTOSECOND MICRO-CARS EXPERIMENTAL APPARATUS

RT/2020/18/ENEA

ITALIAN NATIONAL AGENCY FOR NEW TECHNOLOGIES,
ENERGY AND SUSTAINABLE ECONOMIC DEVELOPMENT

S. GAGLIARDI, M. GHEZELBASH,
M. FALCONIERI

Fusion and Technologies for Nuclear Safety Department
Physical Technologies for Safety and Health Division
Casaccia Research Center, Rome

M. MARROCCO

Department of Energy Technologies and Renewable Sources
Division of Production, Storage and Use of Energy
Laboratory of Processes and Systems Engineering
for Energy Decarbonization
Casaccia Research Center, Rome

C. MERLA

Department of Sustainability of Production and
Territorial Systems and Energy Efficiency
Technologies and Methodologies for Health Protection Division
Biomedical Technologies Laboratory
Casaccia Research Center, Rome

F. RONDINO

Fusion and Technologies for Nuclear Safety Department
Physical Technologies for Safety and Health Division
Micro and Nanostructures Laboratory for Photonics
Casaccia Research Center, Rome

# DESIGN AND OPERATION OF A FEMTOSECOND MICRO-CARS EXPERIMENTAL APPARATUS

RT/2020/18/ENEA

ITALIAN NATIONAL AGENCY FOR NEW TECHNOLOGIES,
ENERGY AND SUSTAINABLE ECONOMIC DEVELOPMENT

# DESIGN AND OPERATION OF A FEMTOSECOND MICRO-CARS EXPERIMENTAL APPARATUS

S. Gagliardi, M. Marrocco, C. Merla, F. Rondino, M. Ghezelbash, M. Falconieri

**Riassunto**

La spettroscopia Raman consente di misurare mappe vibrazionali di campioni con alta risoluzione spaziale, utili per l'identificazione di composti chimici senza l'utilizzo di marcatori. In generale però, le tecniche di Raman spontaneo soffrono di alcuni svantaggi, principalmente dovuti ai bassi livelli di segnale e alla eventuale presenza di segnali di fluorescenza, che possono limitarne l'applicabilità. Per contro, le tecniche di Raman coerente, come ad esempio la diffusione Raman Anti-Stokes coerente (CARS), sfruttando la nonlinearità dell'interazione tra luce di sonda e campione, permettono di superare i limiti sopra descritti, e per questa ragione sono ampiamente utilizzate nonostante la maggior complessità e il costo dell'apparato sperimentale. D'altronde, negli ultimi venti anni, la grande diffusione di oscillatori laser a impulsi ultracorti e la disponibilità di fibre a cristalli fotonici per la generazione di luce bianca coerente hanno facilitato lo sviluppo di microscopi CARS a bassa energia di eccitazione e tempi di acquisizione brevi, che sono di particolare utilità in campo biologico e biomedico. In questo rapporto tecnico, dopo un breve richiamo alle caratteristiche della spettroscopia CARS al femtosecondo, viene descritto il microspettrometro CARS realizzato nel C. R. Casaccia nell'ambito di un progetto ENEA inter-dipartimentale. Inoltre, vengono riportati e discussi i risultati sperimentali ottenuti durante i primi due anni di operatività del sistema.

**Parole chiave:** Multiplex CARS, CARS al femtsecondo, fibra a cristallo fotonico, generazione di supercontinuo, microscopia non lineare.

**Abstract**

*Raman spectroscopy allows the measurement of vibrational maps of samples with high spatial resolution, useful for the identification of chemical compounds without the use of labels. In general, however, spontaneous Raman techniques suffer from some disadvantages, mainly due to low signal levels and the possible presence of fluorescence signals, which can limit their applicability. On the other hand, coherent Raman techniques, such as Coherent Anti-Stokes Raman Scattering (CARS), exploiting the nonlinearity of the interaction between probe and sample light, permit to overcome the limits described above, and for this reason they are widely used despite the greater complexity and cost of the experimental apparatus. On the other hand, in the last twenty years, the great diffusion of ultrashort pulse laser oscillators and the availability of photonic crystal fibers for the generation of coherent white light have facilitated the development of CARS microscopes with low excitation energy and short acquisition times, which are particularly useful in the biological and biomedical fields. In this technical report, after a brief reference to the characteristics of the femtosecond CARS spectroscopy, the CARS microspectrometer made in C. R. Casaccia in the framework of an inter-departmental ENEA project is described. Furthermore, the experimental results obtained during the first two years of operation of the system are reported and discussed.*

***Keywords:*** *Multiplex CARS, femtosecond CARS, photonic crystal fiber, supercontinuum generation, nonlinear microscopy.*

**- Indice**

carattere font 10 - Interlinea: 1,5

## 1. Introduction

All molecules are constituted by two or more atoms bound together, that oscillate around their equilibrium position at specific frequencies, which can be measured by means of spectroscopic techniques exploiting the interactions between matter and light. The molecular vibrational frequencies depend on the atomic masses and on the specific strength of the bonds, and are also affected by both the molecular structure and the surrounding medium, so that the vibrational spectrum gives information on the physical and chemical nature of a sample. The simplest vibrational spectroscopic techniques are based on linear interaction between the electromagnetic field and the matter; they are the infrared spectrophotometry, usually implemented in Fourier-Transform Infra-Red (FTIR) spectrometers, and the Raman scattering. Both these techniques rely on simple experimental set-ups, nowadays commercially available at relatively low cost, but are severely affected by lack of spatial resolution and poor sensibility on non-polar bindings (FTIR), or by the inherent weakness (1 useful photon over about $10^4$) of the signal (for Raman).These drawbacks are particularly relevant in the case of vibrational microscopy, where high sensitivity and high spatial resolution are both necessary to obtain well-defined vibrational images of inhomogeneous specimens.

On the other hand, non-linear spectroscopies can overcome these limitations, and the recent development of reliable and relatively simple ultrafast laser sources, providing the necessary high photon density excitation, is simplifying their application. In particular, Coherent Anti-Stokes Raman Scattering (CARS) allows the study of Raman active modes with some advantages over the corresponding spontaneous (and linear) Raman scattering. First of all, the coherent signal generated in a defined direction is more intense (up to a factor $10^5$) than the corresponding incoherent spontaneous signal. Moreover, the CARS signal is emitted at wavelengths shorter than the excitation spectral region, thus avoiding fluorescence background noise. Furthermore, since the nonlinear process occurs at the focused laser spot, CARS microscopy is inherently confocal. In view of these features, CARS microscopy is presently widely used as a diagnostic tool for a variety of applications ranging from biophysics to material science.

The development of cutting-edge laser-based diagnostic techniques with a high interdisciplinary vocation is a valuable challenge in ENEA, and particularly in the Casaccia Research Center, where a long tradition of ultrafast spectroscopy meets biomedical research and energy technologies.

Within this context, a single-oscillator fs micro-CARS system has been developed in the framework of an internally funded inter-Department project named LINC (Laboratory for INterdisciplinary applications of CARS spectroscopy). The Project started in January 2018, with small investments from ENEA DTE (now TERIN), FSN, and SSPT Departments, and from DTE-PCU, FSN-TECFIS, and SSPT-TECS Divisions, which covered the costs of optical and mechanical components needed for a basic set-up, whose core is constituted by a fs laser source equipped with accessories and diagnostics already available in the FSN-TECFIS ultrafast spectroscopy laboratory operating in the Casaccia Research Center.

It is worth underlining that the whole CARS experimental system, from the feasibility study to component acquisition, realization and test, and data acquisition software, was completely realized ex-novo in the framework of the LINC Project. Moreover, to encourage application in other fields of interest and stimulate contributions, two seminars were given in the Casaccia Research Center to illustrate the Project and its initial outcomes to potentially interested Colleagues.

The first results obtained in the framework of the LINC Project were presented at two editions of the European Conference on Non-Linear Optical Spectroscopy, ECONOS, in 2018 and 2019 and two papers were published on a peer-reviewed international journal [1, 2].

In this report, the basic characteristics of femtosecond micro-CARS systems are described first. Then, the experimental setup and its main constituents are presented. Finally, results on system performance and modeling, as well as measurements on reference samples, are commented. Planned work and future perspectives are drawn in conclusion.

### 1.1 Basic Features of Femtosecond micro-CARS Spectroscopy

CARS spectroscopy is a heterodyne technique based on the interaction between three laser beams, namely the pump, Stokes and probe beams with photon energies $\hbar\omega_{pump}$, $\hbar\omega_{Stokes}$, $\hbar\omega_{probe}$, and a sample having a third-order susceptibility that generates a new electromagnetic wave at anti-Stokes frequency with photon energy $\hbar\omega_{AS} = \hbar(\omega_{pump} - \omega_{Stokes} + \omega_{probe})$. The four-wave mixing process is described by the polarization wave:

$$P^{(3)}(\omega_{AS}) = \chi^{(3)}\left(\omega_{pump}, \omega_{Stokes}, \omega_{probe}\right) E_{pump} E_{probe} E^{*}_{Stokes}$$

where $\chi^{(3)}\left(\omega_{pump}, \omega_{probe}, \omega_{Stokes}\right)$ is the third-order nonlinear susceptibility of the sample, and $E_{pump}, E_{probe}$ and $E^{*}_{Stokes}$ are the electric fields of the interacting beams. The whole process can be represented by the diagram reported in Fig. 1.

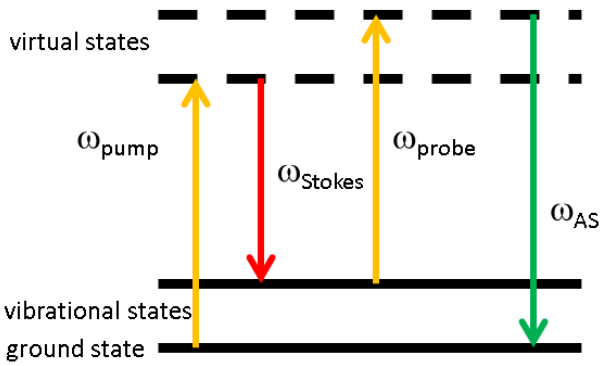


**Figure 1.** Diagram of the (degenerate if $\omega_{pump} = \omega_{probe}$) CARS process.

CARS experiments were at first demonstrated by employing two monochromatic nanosecond lasers, according to the well-known degenerate CARS scheme, where one of the two lasers provides both the pump and the probe excitation and the other is tuned so that the difference $\omega_{pump} - \omega_{Stokes}$ equals a vibrational frequency of the sample [3]. In this way it is possible to monitor a selected chemical bond or to measure the population of a vibrational state thanks to its dependence on temperature. With nanosecond pulsed lasers, the study of a whole vibrational spectrum is possible by collecting successive CARS signals obtained tuning the Stokes beam (scanned CARS); on the other hand, the very same information can be obtained on a single-shot basis with the help of broadband laser sources (broadband CARS). Thanks to recent advances and commercial availability of laser systems with pulse duration of few tens of femtoseconds, various so-called multiplex CARS systems have been developed to study broadband vibrational spectra and their time evolution. Acquisition of frequency and time information is made possible by the characteristics of fs laser pulses that are short enough to follow the time evolution of the molecule under study and, plus, are broad enough to cover the wavelength span of molecular vibrational bands. The energy-level scheme in Fig. 2 depicts typical molecular transitions happening during multiplex CARS interaction [4-7].

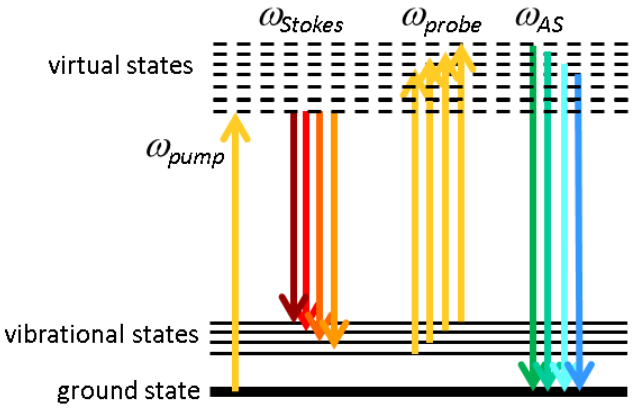


**Figure 2.** Diagram of the multiplex CARS process, involving monochromatic degenerate pump and probe beams, and a wide band Stokes beam, generating a wide band CARS signal.

Despite the attractive features depicted above, in its simplest realization, any conventional femtosecond CARS set-up presents a major drawback for the presence of a strong background due to the non-resonant simultaneous processes (due to competing four-wave mixing phenomena). The background signal, independent from the Raman shift, affects the vibrational lineshapes and reduces the contrast in imaging. In order to overcome this obstacle, a convenient choice is represented by the measurement of the backward-directed signal (epi-detection). This was demonstrated to be less sensitive to the background contribution, being mostly produced by the small inhomogeneities occurring in the sample. What is more, these inhomogeneities, which are better detected in epi-geometry rather than in transmission (or forward-detection), are usually the objective of the sample characterization. Indeed, theoretical calculations and experimental results show that forward- and backward-directed signals are equally intense in case of thin samples, while, for increasing sample thickness, the intensity of the forward signal becomes much larger

than the backward one. It is then evident that any solvent or thick surrounding medium contribution is minimized in epi-detection configuration where the reflected signal originates from the thin section below the sample surface. Experimental results also showed the role of the refractive index mismatch inside the sample which causes backreflection of the forward signal, and can be exploited in microscopy as additional contrast mechanism [8, 9].

As far as the broadband Stokes beam is concerned, in basic multiplex CARS systems this beam can be obtained by the supercontinuum (SC) white-light produced by a highly nonlinear optical fiber (photonic crystal fiber, PCF) which is efficiently excited by ultrashort laser pulses [4-7, 10]. For setups using an unamplified femtosecond oscillator, delivering few nJ, the high fluence necessary for the occurrence of nonlinear optical processes can be only achieved by tightly focusing the beams on the sample using a microscope objective; as a consequence of the generation of the nonlinear signal only in the focal region, thus the so-called micro-CARS systems inherently allow high axial resolution and therefore 3D optical sectioning of thick samples [8, 9].

### 1.2 Supercontinuum generation by photonic crystal fibers

Even though the first demonstration of SC emission from PCF for use as Stokes beam in a femtosecond micro-CARS system was reported in 2004 [4], research is still in progress in order to improve the stability and extend the accessible CARS spectral range, choosing the suitable photonic device and optimizing the excitation conditions [5-7, 10-14].

Essentially, generation of the SC white light in a nonlinear fiber is due to the occurrence of third order processes, mainly self-phase modulation (SPM), four-wave mixing (FWM) and stimulated Raman scattering (SRS). SPM is produced by the intensity dependence of the refractive index (Kerr effect) which introduces a time-dependent phase in the propagating pulse, causing generation of new frequencies. FWM, and specifically degenerate four wave mixing (DFWM), involves generation of two different frequencies following interaction of two beams at the same frequency, while SRS accounts for the interaction of the electromagnetic fields with phonons, producing novel frequencies at the Raman resonances of the fiber material. In a PCF, the photonic crystal structure is engineered to produce a strong field confinement inside a small area core, providing enhancement of the optical nonlinearities.

All the nonlinear processes depicted above are also strongly influenced by the chromatic dispersion (i.e. the dependence of the refractive index on the optical field frequency) of the fiber, and especially DFWM which requires phase matching; besides, also the dispersion properties of the excitation pulse come into play. The latter ones can be somewhat optimized, being determined by the pulse characteristics at the laser output and by the optical elements encountered by the pulse before entering the fiber. As a matter of fact, in common materials the refractive index is higher at shorter wavelengths (normal dispersion), so that, when travelling into the material, the blue wavelengths contained in the pulse spectrum are slowed down more than the red ones, while the opposite situation is realized when the refractive index decreases at shorter wavelengths (anomalous dispersion). In both cases the pulse spectral content is redistributed in time; this phenomenon is

known as chirp, referring to the frequency changes in the bird chirp. The parameter quantifying the chromatic dispersion in materials is the group delay dispersion (GDD, which is positive in case of normal dispersion and negative for anomalous dispersion). In a PCF the dispersion properties can be tailored by purposely designing the photonic crystal microstructure, so that it is possible to realize devices with normal dispersion, monotonic dispersion varying from normal to anomalous with a single zero-dispersion wavelength (ZDW), and also devices with non-monotonic dispersion showing two ZDWs.

The laser excitation characteristics, such as wavelength, power, temporal shape and chirp conditions eventually determine the spectrum and the spectrogram of the SC emission of a given fiber. In particular, it was demonstrated that SC emission from PCF with single ZDW used in the first multiplex CARS experiments was quite noisy and unstable, making very difficult the practical use in vibrational microscopy. This led to the development of devices with two ZDWs, optimized for laser excitation wavelength lying between them in the anomalous spectral region, whose SC emission is much more stable. The SC emitted by this kind of PCF is characterized by two broad bands, one in the visible region spanning from about 600 nm to 800 nm, and the other in the infrared part, ranging between about 900 and 1200 nm, which is the one actually used as broadband Stokes beam in multiplex CARS experiments [10, 15, 16].

## 2. Experimental apparatus

The experimental set-up used in this work is typical for single-laser oscillator multiplex CARS arrangements [4]; the optical layout is shown in Fig. 3 and in the following we give a brief description of its principle of operation and of its main constituents. A picture of the realized system is reported in Fig. 4.

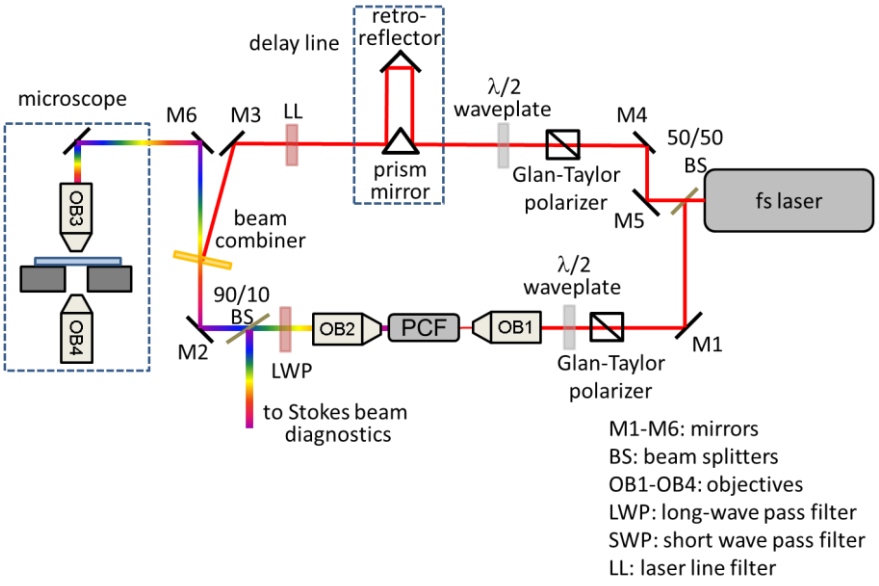


**Figure 3.** Scheme of the micro-CARS set-up.

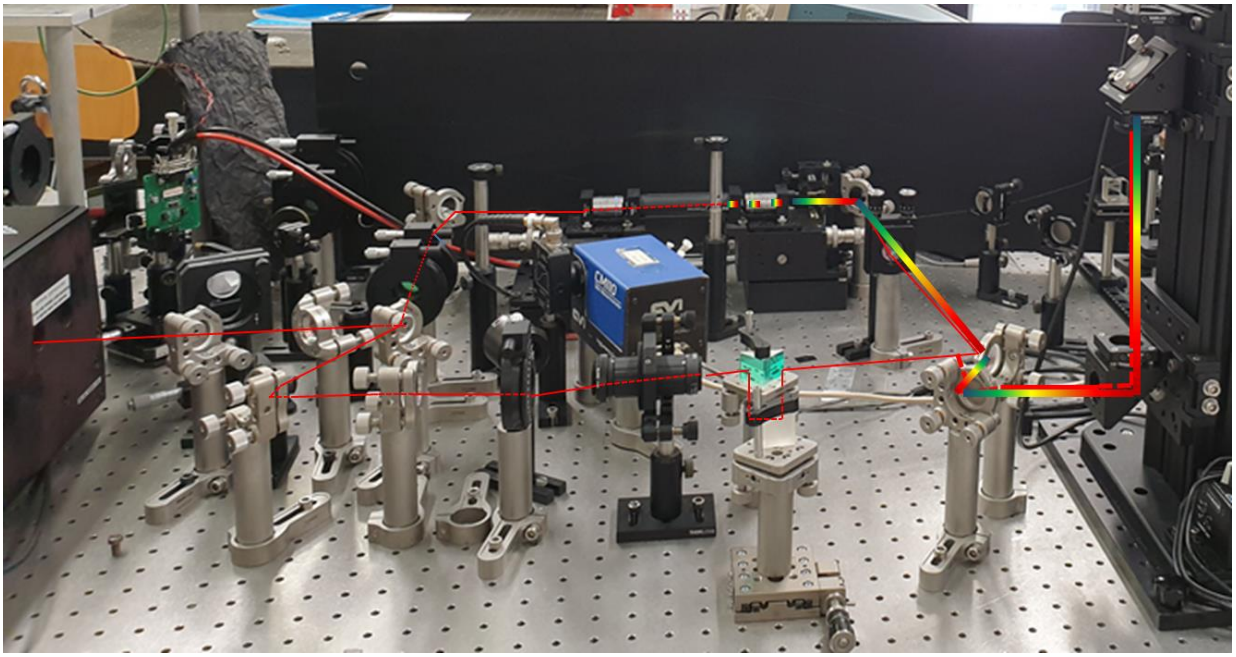

**Figure 4.** Picture of the realized micro-CARS system.

### 2.1 The femtosecond laser

The oscillator used in the experimental set-up is a Coherent MIRA 900 F, which is a mode-locked tunable ultrafast laser based on a Titanium:sapphire gain medium. The energy needed for the MIRA lasing has to be provided by a green pump laser, a Coherent VERDI V7 operating at 6.10 W output power in the present case. The MIRA is equipped with broadband optics allowing continuous tunability in the 720-1000 nm range.

In order to obtain ultrashort pulses, the MIRA exploits the passive mode-locking technique based on the self-Kerr lens effect, where a variable loss is introduced in the cavity to force the formation of high peak power pulses due to constructive interference among modes. The MIRA cavity is designed to produce 100 fs pulses spaced by 13.2 ns, corresponding to a laser repetition rate equal to 76 MHz, with about 10 nJ pulse energy.

Since ultrashort pulses travel through different optical elements in the cavity and in the experimental setup, they are subjected to dispersion due to their intrinsic bandwidth and to the wavelength dependence of the optics refractive index. In order to compensate for the dispersive elements encountered in the propagation and to attain a minimum pulse duration, the MIRA cavity is equipped with a pulse compressor capable to add negative dispersion. Pulses without chirp satisfy the minimum time-bandwidth product condition and are called transform-limited; in principle, this condition is desirable, but MIRA lasing is poorly stable for very small pulse chirp, and stable in a wider region with positive chirp. For diagnostics purpose, the oscillator pulsewidth can be measured by an instrument called autocorrelator (an APE PulseCheck apparatus in our case), which exploits the dependence of the intensity of the second harmonic generated in a nonlinear

crystal on the temporal superposition of two pulses derived from the same laser beam. The laser bandwidth can be easily measured using a spectrometer, thus providing a complete characterization of the laser beam.

### 2.2 The optical layout

Pulses emitted from the oscillator at 780 nm are divided by a 50/50 beamsplitter in two beams; one beam, after passing through a variable attenuator composed by a λ/2 waveplate/polarizer couple, is focused by a 40x objective (Olympus Plan Achromat) to the input of a FemtoWHITE CARS® (NKT Photonics) PCF to produce the infrared supercontinuum to be used as Stokes beam. The FemtoWHITE CARS is a 12 cm long fiber with two zero dispersion wavelengths, at 775 nm and 945 nm, optimized to be excited at wavelengths between the two extremes of zero dispersion.

The output of the fiber is collimated by a 20x objective (Olympus Plan Achromat) and its infrared part, used for the Stokes beam, is selected by a long-wave pass filter with cutoff at 800 nm (Melles Griot); a beam splitter placed after the fiber collimation objective offers the possibility to measure the beam spectrum while detecting the CARS signal. The spectral width of the Stokes beam goes roughly from 900 nm to 1150 nm, depending on the PCF excitation conditions, as detailed below; considering the pump/probe beam wavelength equal to 780 nm, the obtained accessible vibrational region is from about 1700 $cm^{-1}$ to more than 4000 $cm^{-1}$. Maximum pulse energy at the fiber launching objective is about 4 nJ and the coupling efficiency (ratio of the power after the collimation objective to the power at the launching objective) is around 40%. The other portion of the laser pulses, after passing through a variable beam expander, a variable attenuator, a delay line, and a 3 nm bandpass filter (Semrock LL01-780-25 MaxLine®), is combined by a dichroic mirror (Semrock LP02-780RU-25 RazorEdge®) with the PCF output. The role of the variable beam expander in the pump/probe arm is to improve the beam mode-matching with the Stokes beam; as a matter of fact, to obtain optimized nonlinear interaction in the sample the two beams must be focused at the same depth and have the same spot size. Maximum energy of the pump plus probe beam is 1.2 nJ after the 3 nm bandpass filter. The two beams are routed to a home-made microscope, and finally focused onto the sample.

Alignment of the system consisted in achieving optimal spatial superposition and mode-matching of the pump/probe and Stokes beams in the sample, in achieving temporal coincidence of the pulses in the interaction zone, and in optimization of the collection of the CARS signal by alignment of the microscope optics. The spatial superposition and the spatial mode matching of the beams are controlled by the steering mirrors and by the variable beam expander respectively in the pump/probe arm. The variable beam expander and the recollimation objective at the PCF exit also control the beam diameter at the microscope objective entrance pupil, permitting optimal focusing. The temporal coincidence of both pump/probe pulses and Stokes ones is also necessary, and is accomplished by the presence of the variable delay line in the pump/probe arm; small adjustments of the delay between the beams also permits to optimize the CARS signal at a given Raman shift (enabling application of spectral focusing as soon as pump and Stokes pulses have similar chirp), as the Stokes beam is strongly chirped.

### 2.3 The microscope

The pump/probe and Stokes beams are focused onto the sample through a home-built microscope, purposely designed and realized with commercial discrete components. The scheme and a picture of the microscope are reported in Fig. 5. Briefly, an entrance periscope allows to route the excitation beams onto a dichroic beamsplitter (Semrock LP02-780RU-25 RazorEdge®) which reflects them into the focusing objective, mounted on a turret. The sample is mounted on a computer-controlled motorized stage allowing positioning of the sample with a resolution better than 1-μm, as well as measurement of vibrational maps. The CARS signal can be collected in forward configuration by a second 20x (Leitz Wetzlar) objective placed below the sample or, in backward configuration, by the same focusing objective (epi-configuration). The forward-collected signal is filtered by a long-wave pass edge filter (Semrock SP01-785RU-25 RazorEdge®) and launched into a fiber to be delivered to one of the detection systems available for the experiment and described below, while in the epi-configuration the collected signal is fiber-launched after rejection of the excitation beam by the dichroic beamsplitter. In both configurations, further attenuation of the excitation components is achieved with a combination of a long-wave pass filter and a short-wave pass one, allowing only the anti-Stokes 600÷750 nm range (roughly the Raman shift interval between 500 and 3000 $cm^{-1}$) to reach the detectors.

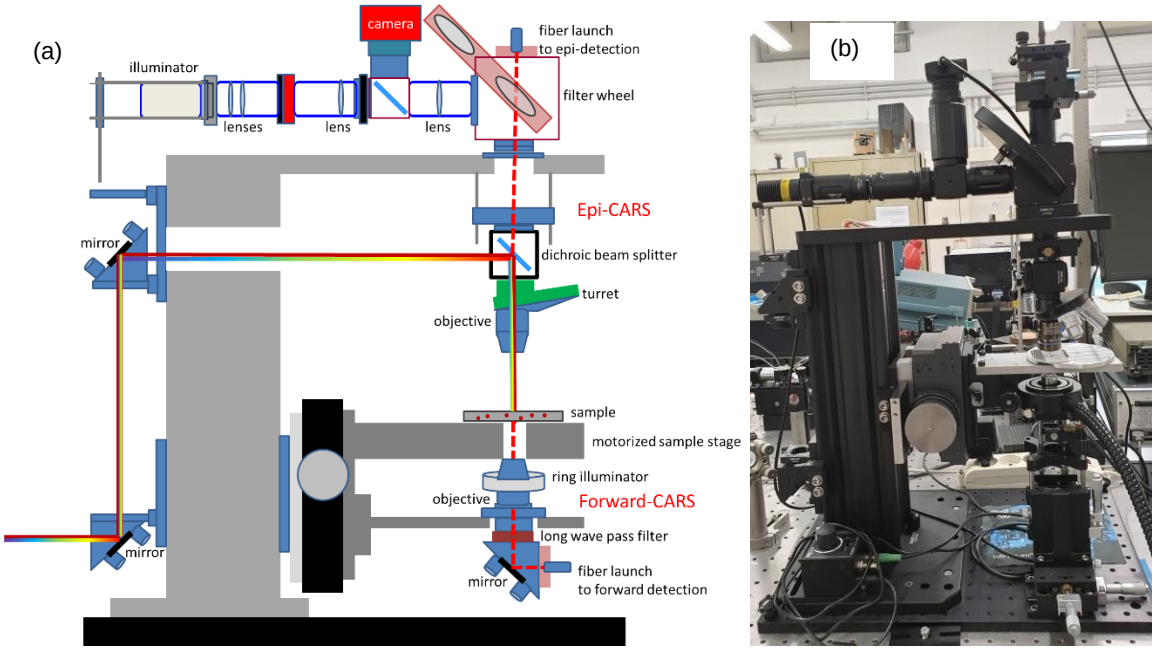


**Figure 5.** Microscope scheme (a) and picture (b).

Two different microscope objectives were used here to focus the excitation beams onto the samples: a long working distance metallographic Leitz 32x and a Nikon 50x optimized for multiphoton applications.

The microscope is also equipped with a camera for optical imaging of the sample and two illuminators, providing both retroreflected and transmitted sample illumination, which ensure clear imaging of both non-transparent and poorly contrasted transparent samples. The real-time imaging of the sample also permits to visualize the position of the excitation beams, providing the possibility of exact superposition of the optical image of the sample to its CARS map. Alignment of the microscope consisted in optimizing the illumination

of the focusing objective pupil using the entrance periscope and in optimizing the CARS signal collection. In forward configuration the latter operation consisted in the alignment of the collection objective/fiber launch assembly placed below the sample (see Fig. 5), while in epi-collection only the fiber launch had to be optimized.

### 2.4 The signal detection systems

Two different systems were set up for detection of the CARS signal. The first one is based on a monochromator/detector assembly composed by a Horiba/Jobin Yvon TRIAX 320 monochromator and by a thermoelectrically cooled Andor Newton intensified CCD. This system allows for multichannel measurements and is therefore suitable for hyperspectral imaging. The second system is based on a double monochromator (Solar MSA 130) coupled to a thermoelectrically cooled Hamamatsu photomultiplier (R943-02 model). The output of the photomultiplier is read in photon-counting mode by a Becker&Hickl multiscaler card (PMS-400-A). This system is suitable for fast measurement of selected single spectral CARS lines, i.e. for vibrational maps of specific bonds. Both the detection systems are controlled by a PC using their proprietary software and LabVIEW virtual instruments expressly developed within the framework of this activity.

## 3. Results

### 3.1 Supercontinuum beam experimental characterization

As the operation conditions determine the PCF emission, which ultimately influence the measured CARS signal, characterization of the SC spectrum was performed, at fixed excitation wavelength (780 nm) in different pulse chirp and power conditions.

A first characterization of the PCF SC emission was performed in the whole beam wavelength range, using two different Horiba Jobin-Yvon systems: a silicon CCD coupled to a Triax 550 monochromator, for the visible region (600-950 nm) and a Symphony InGaAs CCD coupled to an iHR 320 monochromator (courtesy of Dr. Mario Tucci ENEA TERIN-FSN-TEF) for the near-infrared portion (900-1200 nm). The two data sets, after calibration for correction of system responses, were then merged using the overlapped portion and finally the spectral power density of the resulting complete spectrum was normalized using the measured power at the PCF output. Later, owing to the discontinuous availability of the InGaAs CCD, a different system based on a small monochromator (Instrument Division CM110) coupled to an InGaAs photodiode with lock-in signal detection was set up. The system was interfaced to a PC and a dedicated software, written in LabVIEW environment, allows the acquisition of the Stokes spectrum from 900 nm to 1200 nm in approximately 30 seconds, with 5 nm resolution.

Different working conditions of the PCF were achieved essentially by varying the incident power adjusting the variable attenuator, and by varying the beam chirp at the fiber input. In particular, the laser oscillator intracavity prism compressor was used to change the pulse duration and the chirp condition of the excitation

pulse; furthermore, a purposely-built prism compressor was used in the optical layout to introduce a negative GDD thus compensating or over-compensating the optical components of the set up with normal dispersion (the main contribution coming from the components of the variable attenuator and the PCF coupling objective). The laser output pulses were fully characterized by measurements of time duration and bandwidth, then the chirp conditions at the PCF input were obtained from the value of the GDD of the layout dispersive elements, and from the prism compressor parameters [17]. An independent indication on the laser chirp conditions was given by the measured values of the pulse duration at the PCF input objective. The SC spectra in different conditions (summarized in Table I) were measured after maximization of the fiber output obtained by careful alignment of the PCF launching objective.

**Table I.** Pulse bandwidth, durations and chirp conditions for different optical configurations.

| **$\Delta\omega$@laser exit port (nm)** | **$\tau_{exp}$@laser exit port (fs)** | **$\tau_{exp}$@PCF input objective (fs)** | **chirp** |
|---|---|---|---|
| 8.9 | 101 | 200 | >0 |
| 8.9 | 101 | 223 | ≈0 |
| 7.4 | 169 | 298 | <0 |

The resulting measured spectra under transform-limited, positively or negatively chirped beam excitation with different average power values are reported in Fig. 6.

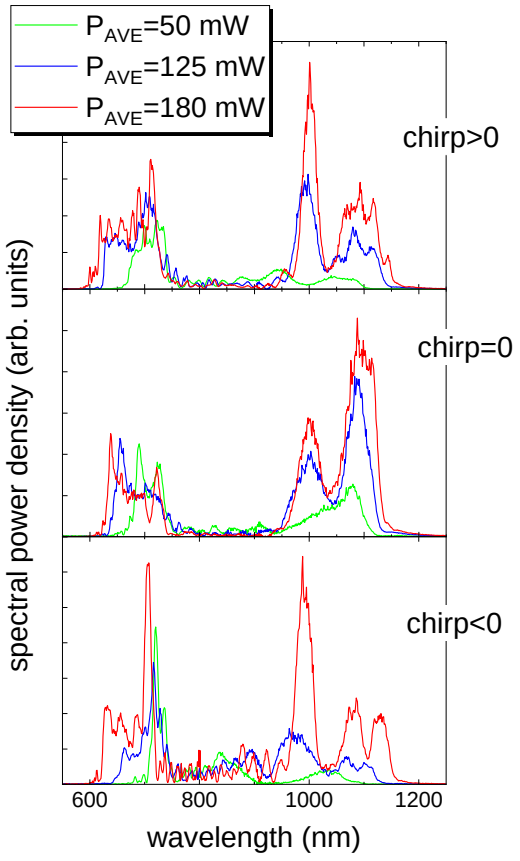


**Figure 6.** Experimental SC spectra, at different beam chirp and laser power conditions (average power $P_{AVE}$).

The experimental SC spectra (Fig. 6) are mainly constituted by two bands at visible and near-infrared (near-IR) wavelengths, separated by a depleted region around the excitation wavelength with a clear broadening for increasing laser average power. At the maximum power the visible bandwidth is about 100 nm, whereas the near-IR band is about 200 nm wide and presents some finer structures with two main peaks around 1000 and 1100 nm. The experimental data show that positive and negative chirp conditions produce a quite similar emission spectrum, apart from minor differences like the presence of a more pronounced peak at 700 nm for negative GDD, as already reported in [1]. On the other hand, an important difference is instead found for unchirped excitation conditions. In particular, in the near infrared region, which is the spectral region actually exploited as Stokes beam for CARS measurements, it is possible to observe that the relative ratio between the intensities of the main peaks at 1000 and 1100 nm is reversed when chirp approaches zero. This gives the opportunity to trim the Stokes spectrum according to the Raman spectral region of interest [1] in the CARS experiment. In fact, when using a pump/probe beam at 780 nm, the 1000 nm Stokes band probes the lipid band at 2800 $cm^{-1}$, while the broader 1100 nm band is suitable to investigate the 3200-3700 $cm^{-1}$ Raman band.

### 3.2 Forward-CARS signal detection

The set-up was initially aligned and tested measuring the CARS spectrum of a reference sample (cyclohexane) contained in a quartz cuvette in forward detection, using the TRIAX320/Andor Newton intensified CCD assembly. After alignment and optimization of the setup, the acquisition time of a very intense CARS spectrum resulted on the order of a fraction of second, depending on the monochromator entrance slit, i.e. using the 50x objective, the maximum signal intensity was around 5000 counts with entrance slit of 10 μm and an acquisition time of 0.1 s.

In a first set of experiments, the cyclohexane CARS signal was measured simultaneously with the Stokes beam spectrum in order to establish the best PCF excitation conditions for accurate measurements. For comparison, a reference cyclohexane Raman spectrum was measured using a spontaneous Raman spectrometer with CW 532 nm laser excitation. The results shown in Fig. 7 demonstrate that the CARS spectrum is "shaped" by the Stokes one, as expected since the CARS signal depends linearly on the Stokes spectral energy density. Therefore, if the Stokes beam is not spectrally flat in the wavelength region of interest, the CARS spectrum can be strongly deformed; from Fig. 7 it is evident that the Stokes beam obtained by PCF excitation with low laser beam chirp is clearly more suitable for CARS signals around 2800 $cm^{-1}$. On the contrary, using chirped laser excitation the relative intensity of the two cyclohexane peaks is strongly altered in comparison to the reference spectrum. Comparison with spontaneous Raman spectrum also shows an evident broadening of the peaks: the full width half maximum (FWHM) of the spontaneous Raman peak centered at 2850 $cm^{-1}$ is 10 $cm^{-1}$, depending on both the intrinsic linewidth and broadening due

to the spectrometer, while the FWHM of the same CARS line is 60 $cm^{-1}$, mainly due to the large bandwidth of the pump/probe beam, which, after the bandpass filter, is 3 nm wide (i.e. 50 $cm^{-1}$).

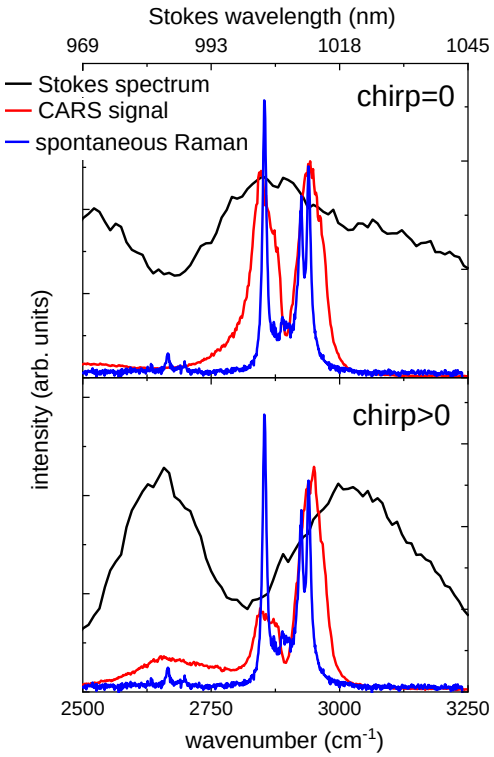


**Figure 7.** Stokes beam and corresponding cyclohexane CARS spectra produced with pulses with different beam chirp conditions at the PCF input; also shown the spontaneous cyclohexane Raman spectrum.

### 3.3 Stability of the system

As described above, the SC beam is generated in the PCF by nonlinear processes which are inherently critically dependent on the working conditions [1-2, 18-19]. Indeed, the CARS signal is proportional to the intensity of the Stokes spectrum at the corresponding wavelength, so the stability of the SC emission also affects the stability of the CARS signal. Furthermore, SC generation in the PCF is strongly affected by the coupling efficiency of the launching objective, because of the nonlinearity of the generation processes. Therefore, even small misalignments due to mechanical instabilities or thermal drifts produce large effects on the PCF emission spectrum, which ultimately affects the measured CARS spectrum as shown above. Great care was thus taken in the realization of the experimental setup to minimize instabilities and sensitivity to ambient fluctuations: the whole system is mounted on a vibration insulated 12" thick honeycomb optical table, and the launching objective-fiber assembly is mounted on a Thorlabs Nanomax® flexure stage providing three-axis adjustment with differential actuators. Despite these precautions, during system operation the SC spectrum was observed to show fluctuations on the timescale of some tens of seconds. Thus, a systematic study of the IR spectrum of the SC emission (Stokes beam) was performed and statistical

methods were applied to gain information on both overall spectral characteristics and stability and the dependence on laser excitation conditions.

As depicted above, the positive and negative chirp conditions of the excitation beam resulted in very similar SC spectra, so that systematic studies were only performed in different positive chirp conditions, quantified by the ratio, *R*, of the measured time-bandwidth product to that of transform-limited pulses, i.e. 0.315 for $sech^2$ pulses. In this manner, it was possible to remove the prism compressor from the optical layout, thus shortening the optical path and simplifying the system. The different chirp conditions were practically attained by altering the laser intracavity pulse compressor, and fully characterized at the laser exit port by time duration and bandwidth measurements. The values of *R* calculated in the different conditions span from 1.5 up to 1.9. The effect of the pulse propagation through the optical set-up, which resulted in the broadening of the time duration due to the positive GDD added by the dispersive elements, was disregarded as it was constant in the experiment.

The infrared SC spectrum was repeatedly measured with the monochromator/InGaAs photodiode assembly for 5 times at each laser power and chirp condition, ensuring a careful alignment before each measurement. After the measurements, the center of mass (COM) and the width of the spectra were obtained by calculating the first and second momenta (the expected value and the standard deviation σ around the COM, respectively) of the intensity distribution, and are reported in Fig. 8 as a function of the chirp parameter *R* and the laser peak power. Figure 8 shows that, as expected, the COM shifts to longer wavelengths for increasing power and that longer wavelengths are achieved at low chirp conditions. Furthermore, it can be seen that for low and high values of *R* the COM power dependence is stronger than that attained at intermediate chirp conditions. It is also evident that the width of the Stokes beam is larger at low chirp values, so that for multiplex CARS application this excitation condition appears be the most appropriate. On the other hand, at intermediate values of chirp, the Stokes spectra show a well-defined band, suitable for CARS imaging at fixed wavelength.

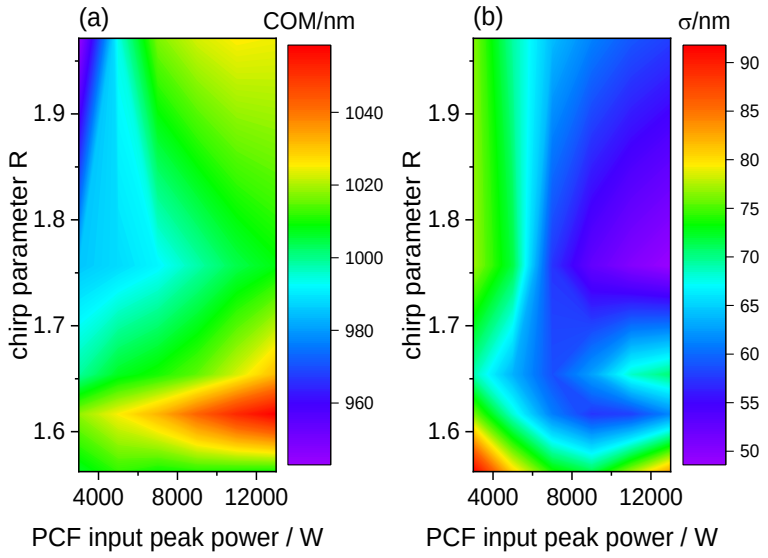


**Figure 8.** Center of mass (COM) (a) and standard deviation around COM (b) of the Stokes beam as function of laser beam chirp parameter *R*, and PCF input peak power.

In order to define robust procedures for CARS measurements requiring extended acquisition time, such as maps or kinetic characterizations, evaluation of the time stability of the system is necessary. To this aim, a statistical descriptor, the Allan variance [20], can be used to quantify the long-time stability of the Stokes beam and of the CARS signal. The signal intensity of the Stokes beam at 1016 nm and of the corresponding CARS signal at 633 nm, were repeatedly measured, every 20 s for 20 minutes at the maximum laser excitation power at positive chirp condition ($R$=1.54) and the Allan variance was calculated according to [21]. The results are reported in Fig. 9a and show that the curves related to Stokes and CARS signal have the very same behavior, confirming that the CARS instability is mainly caused by the SC fluctuations.

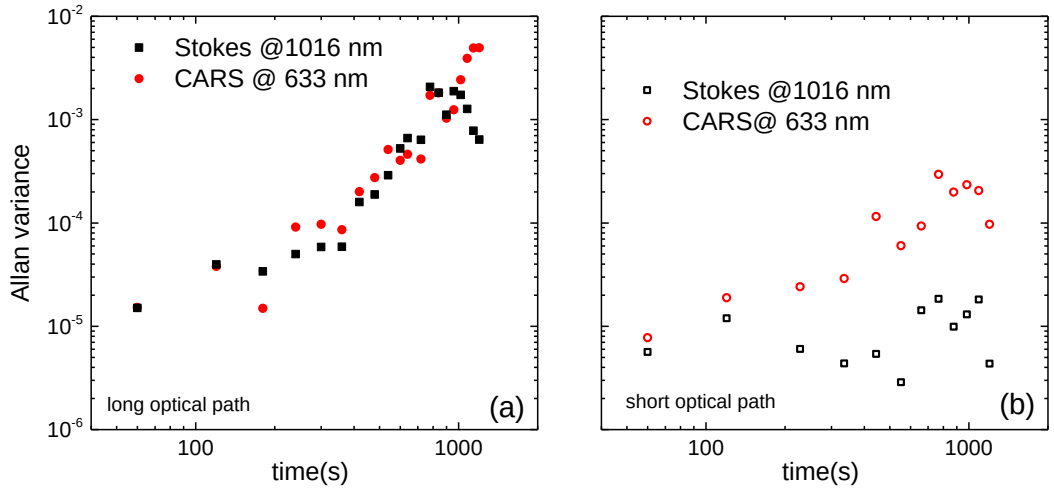


**Figure 9.** Allan variance calculated for Stokes beam and CARS, in the set-up with long optical path (L≈160 cm from the laser exit port to the PCF launching objective) (a); and short optical path (L≈60 cm) (b).

The long-time noise studied in this work is referred to as the technical one; since it is caused by the amplification of the fluctuations of the input laser pulse characteristics, it is always present and is unavoidable despite the care taken in the experimental set-up [2, 18-19]; nevertheless, an attempt to reduce instability was made modifying the set-up by shortening the optical path of the laser excitation pulse. A new set of measurements were performed with the modified set-up and the calculated Allan variance resulted significantly smaller than that obtained in previous conditions, as shown in Fig. 9b. It is worth to note that in this case the trend of the Stokes and CARS curves is not really the same and the CARS signal shows a larger instability. So it can be argued that, while for long optical path the CARS signal instability is essentially caused by the Stokes beam one, with shorter path the decreased instability of the Stokes beam has a lower effect on the noise of the CARS signal, moreover the different shapes of the two curves also suggest different noise origins.

Furthermore, the correlation between the laser chirp conditions and the Stokes beam time-stability was investigated by repeated measurements of the Stokes beam at 1016 nm in different chirp conditions, achieved as described in section 3.1, and calculating the Allan variance, reported in Fig.10. The time stability of the Stokes beam is better at the highest value of $R$, even though deteriorates rapidly, indicating

that this laser excitation condition could help in short-time measurements; on the other hand, for the lowest value of *R*, the slope of the curve is flatter than in the other conditions, so this working condition is suitable for extended time measurements.

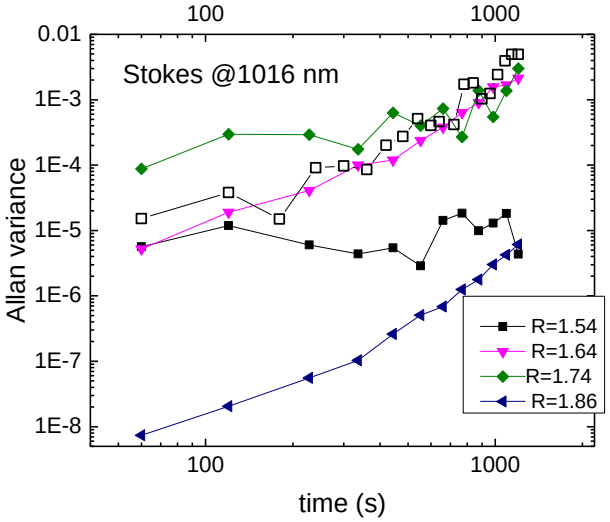


**Figure 10.** Allan variance of the Stokes beam at 1016 nm (a) and of the CARS signal at 633 nm (Raman shift 2977 $cm^{-1}$) (b) in different laser chirp conditions.

### 3.4 Epi- CARS detection

As described above, the epi-detection configuration was also implemented in the microscope and tested on a scotch tape sample placed on a glass substrate. Scotch tape is a quite flat, homogeneous polymeric sample, whose spontaneous Raman spectrum shows an intense vibrational peak around 2960 $cm^{-1}$ due to the stretching modes of CH bonds [22].

The intensity of the CARS signal of this peak was used to align and optimize the epi-configuration. The first step was the acquisition of the CARS spectrum with the monochromator/CCD detection system, the optimized epi-CARS spectrum, reported in Fig. 11, shows as expected the intense peak around 2960 $cm^{-1}$.

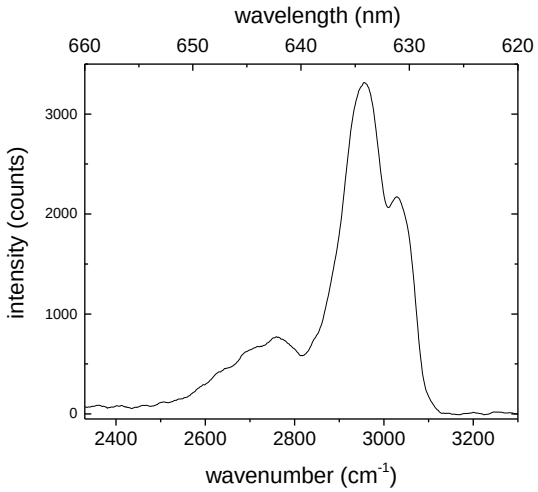


**Figure 11.** CARS spectrum of tape revealed in epi- configuration.

Then, the signal was delivered to the acquisition system based on the double monochromator coupled to the Hamamatsu photomultiplier for the measurement of a vibrational map at 634 nm, corresponding to a Raman shift equal to 2960 $cm^{-1}$. A sample region near the edge of the tape was selected using the optical imaging from the microscope camera, and a 10x10 points, 2 μm spaced, CARS map was acquired with spectral resolution of resolution of 6 nm. The CARS map is reported in Fig. 12 with the CARS signal intensity represented in false colors, together with the corresponding optical image of the sample. The CARS map clearly allows for the distinction between glass and the polymeric sample; furthermore, the CARS image well reproduces the features of the sample, highlighting the edge and the irregularity visible in the optical image. The signal profile at y=6 μm reported in Fig. 12 highlights the step behavior, with a width of 5 μm calculated from the FWHM of the first derivative of the best fit, which can be assumed as the radial resolution of the chemical mapping. This first measurement of the spatial resolution of the system relies on the hypothesis of an ideally sharp edge of the scotch tape, which was however not characterized by an independent measurement, so this result is still to be confirmed and has to be considered as preliminary.

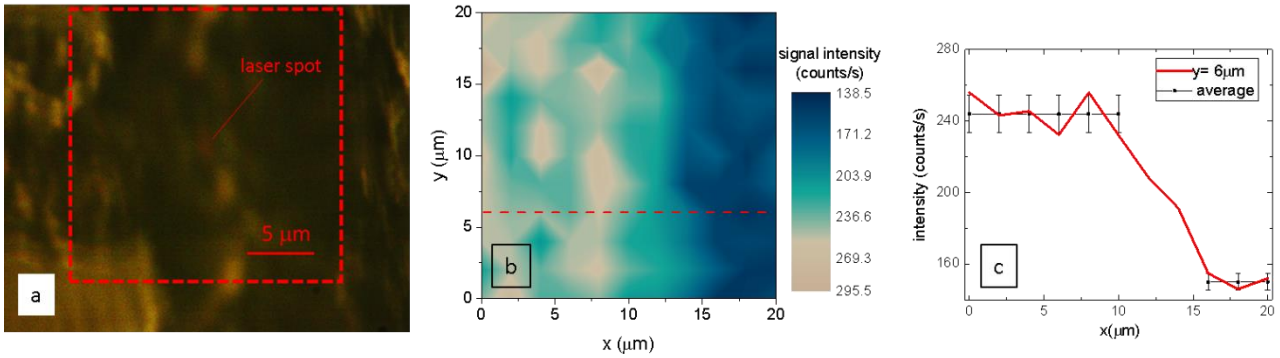


**Figure 12.** Optical image of the edge of the tape (a), CARS map of the CH bonds (b), intensity profile at fixed y value (c).

### 3.5 Supercontinuum modeling

As described above, the SC generation is strictly related to the excitation conditions, so that even small variations of the latter induce relevant modifications of the emitted spectrum, which ultimately affect the CARS signal. Selection of the most suitable PCF excitation conditions is a time-consuming task, that can be simplified with the help of computer modeling. Thus, in the attempt to set up a tool useful in the selection of the optimal fiber working conditions, we implemented a numerical model of our PCF based on a freely available MATLAB® [23] code for the calculation of the generated SC beam.

The model is based on the solution of the equation describing the laser pulse propagation in a dispersive and nonlinear medium. The laser pulse is described by its electric field:

$$E(r,t) = \frac{1}{2}\{E(x,y,z,t)e^{i\omega_0 t} + cc\} \quad (1)$$

which can be written in the frequency-domain through the Fourier transform in terms of its complex spectral envelope *A(z, ω)*:

$$\tilde{E}(r,\omega) = F(x,y,\omega)\tilde{A}(z,\omega-\omega_0)e^{ik_0 z} \quad (2)$$

The propagation of the laser pulse in the medium (i.e. the fiber) can be calculated by the equation describing the evolution of the envelope *A* in a reference frame moving at the group velocity, assuming a spectral bandwidth small respect to the carrier frequency $\omega_0$ [24]:

$$\frac{\partial A}{\partial z} - \sum_{K>2}\frac{i^{k+1}}{k!}\beta_k\frac{\partial^k A}{\partial t^k} + \frac{\alpha}{2}A = i\gamma\left(1 + i\tau_{shock}\frac{\partial}{\partial T}\right)A\int_{-\infty}^{\infty}|A|^2\,R(T')dT' \quad (3)$$

The equation (3) is referred to as generalized nonlinear Schrödinger equation (GNLSE); the left hand side of the equation describes the linear propagation effects: dispersion phenomena (time-derivative terms) and losses (linear term in *A*), where $\beta_k = \left(\frac{d^k\beta}{d\omega^k}\right)$ are the coefficients of the Taylor expansion of the dispersion curve of the PCF $\beta(\omega)=n(\omega)\omega/c$ around $\omega_0$ and $\alpha$ is the linear power attenuation. The right hand side of the equation (3) models the nonlinear effects, where $\gamma = \frac{\omega_0 n_2(\omega_0)}{cA_{eff}(\omega_0)}$ is the fiber nonlinear coefficient, which is proportional to its nonlinear refractive index $n_2(\omega_0)$, and inversely proportional to the mode effective area in the fiber core $A_{eff}(\omega_0)$; the time derivative term describes the dispersion of the nonlinearity, which is responsible for the occurrence of self-steepening and optical shock formation, on the time scale of $\tau_{shock} = 1/\omega_0$. *R(t)* is the fiber material nonlinear response function which includes both instantaneous electronic and delayed nuclear contributions. Usually, the nonlinear response function is written as:

$$R(t) = (1-f_R)\delta(t) + f_R h_R(t) = (1-f_R)\delta(t) + f_R\frac{\tau_1^2+\tau_2^2}{\tau_1\tau_2^2}e^{-t/\tau_2}\sin(t/\tau_1)\Theta(t) \quad (4)$$

where $f_R$ is the fractional contribution of the delayed Raman response, $\tau_1$ is the reciprocal of the Raman mode frequency and $\tau_2$ its damping time, $\delta(t)$ is the Dirac delta function and $\Theta(t)$ is the Heaviside step

function. Numerical solutions of the GNLSE were demonstrated to successfully model SC emission in a wide variety of parameters.

In order to describe the FemtoWHITE CARS fiber used in our setup, the fiber losses were neglected, while the Raman response parameters of the silica core where taken from the literature ($f_R$=0.18, $\tau_1$=12.2 fs, and $\tau_2$=32 fs). The nonlinear coefficient $\gamma$ and the dispersion parameters were taken from the fiber data sheet as supplied by the manufacturer. In particular, the dispersion curve was fitted with a polynomial function and the resulting parameters used to calculate the coefficients of the Taylor expansion (up to the tenth order) of the dispersion curve used in the model.

In the preliminary simulations, the laser pulse was described using a Gaussian shape characterized by the peak power $P_P$ and transform-limited pulse duration $\tau_{TL}$, calculated from the measured beam average power, and from the measured bandwidth $\Delta\omega$ using the relationship $\tau_{TL}\Delta\omega$=0.44. Under these assumptions, however, the simulated spectra poorly reproduced the experimental ones; this result was somehow expected as the detailed temporal shape of the beam and its chirp are known to strongly influence the SC emission. Thus, we adopted a more realistic description of the femtosecond laser pulse, which, being emitted from a self-Kerr lens mode-locked oscillator, can be more accurately described by a chirped hyperbolic secant function:

$$E(t) = \sqrt{P_P}\,\mathrm{sech}\left(\frac{t}{\tau_0}\right)\exp\left(-\frac{iCt^2}{\tau_0^2}\right) \qquad (5)$$

Thus, the pulses at the laser exit port were characterized by measuring the pulse bandwidth and duration and by the calculated value of the chirp parameter:

$$C = \sqrt{\left(\frac{\tau}{\tau_0}\right)^2 - 1} \qquad [22] \qquad (6)$$

It is to note that this expression is exact in the assumption of Gaussian fields but provides indicative values for fields described by the hyperbolic secant dependence used here. To describe the beam at the fiber input, the effects of the propagation in the optical set-up were then accounted for, calculating the broadening of the pulse duration due to the propagation in the optical elements and the shortening caused by propagation in the prism compressor. The resulting pulse duration was then used to calculate the new chirp parameter (at constant bandwidth) and hence describe the *sech* field fed into the model simulating the SC generation. The simulated spectra, reported in Fig. 13, qualitatively describe well the two branches of the measured SC spectra reported in Fig. 6, separated by a depletion region around the excitation wavelength, even if the visible region is reproduced with a rougher detail. On the other hand, the infrared spectral features are quite similar to the experimental ones, with the evolution of the main bands at 1000 and 1100 nm for different chirp conditions correctly predicted. It was observed that the long-wavelength cut-off was not exactly reproduced using the coefficients obtained from the dispersion curve and only their substantial variation allowed the correct reproduction of this spectral feature. A possible explanation can be ascribed to the

uncertainty of the dispersion curve, which actually describes an average behavior of similar devices, but was not measured for the specific PCF used in this work.

Furthermore, even though the mixed approach applied here, with hyperbolic secant shape and Gaussian chirp, is widely used in the literature, the simulations still show the necessity of a more accurate description of the PCF excitation beam. Work is in progress to implement a model based on a chirped pure-hyperbolic secant pulse shape, allowing for a more realistic description of the laser beam and of the effects of the optical setup on the pulse characteristics.

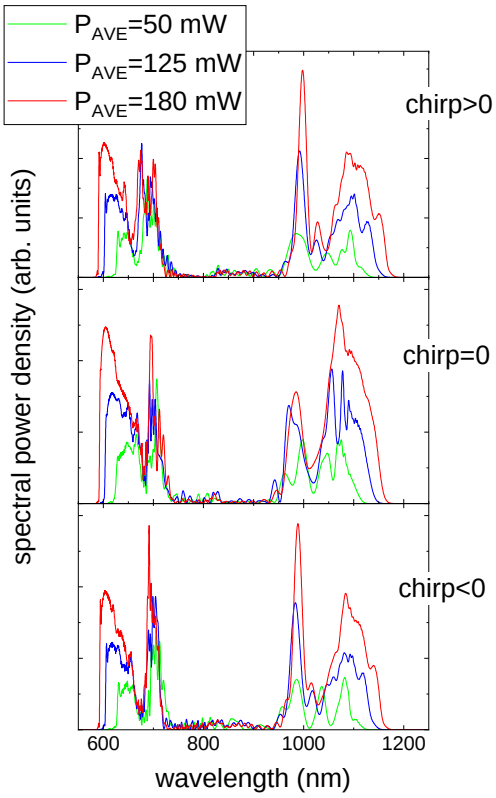


**Figure 13.** Simulated SC spectra, at different beam chirp and laser power conditions (average power $P_{AVE}$).

## 4. Conclusions and perspectives

In the framework of the ENEA interdepartmental LINC project, a single-oscillator femtosecond multiplex micro-CARS system was realized ex-novo, exploiting the fs laser source already present in the FSN-TECFIS Casaccia laboratory and procuring the optomechanical components necessary to complete the optical setup and realize a CARS microscope. The alignment procedures and working conditions, mainly related to the use of the supercontinuum emission from a photonic crystal fiber, were established, and the system performances were assessed both in forward detection configuration, suitable for studying homogeneous samples, and backscattered (epi-) configuration, preferable for chemical mapping of inhomogeneous samples.

In particular, much effort was devoted to the study of the supercontinuum emission generated by the PCF, since its spectral features and stability determine the reshaping of the CARS spectrum and the CARS signal stability which ultimately affects the reliability of a chemical map. Numerical simulations and experimental characterizations were performed to fully characterize the PCF emission in different working conditions, in order to provide a Stokes beam tailored to the particular CARS application.

The spectral and the spatial radial resolution of the system were obtained from CARS measurements on reference samples, i.e. a liquid solvent and the edge of an adhesive transparent tape; finally, the time stability of the system was studied, by means of a statistical descriptor, the Allan variance, in a time frame of 20 minute, an order of magnitude consistent with maps acquisition time for such systems.

Presently, the system can measure CARS spectra at fixed sample position, or, alternatively, can map a signal intensity at fixed wavelength. In order to enable hyperspectral imaging of a sample, it is necessary to implement the system automation program to measure point to point a whole CARS spectrum with a multichannel detection system. Furthermore, the axial and radial resolution of the system will be assessed by mapping purposely prepared samples, made of well dispersed scatterers of known dimension immersed in water and other solvents. Finally, the set-up will be made available for experiments regarding the areas of interest of the ENEA Departments, with special attention to biological samples such as cells or tissues, as those coming from biomedical and agri-food activities, or from bioreactors, but with possible uses for characterization of polymers or lipids in the field of materials science.

**Acknowledgments**

This work was performed in the framework of LINC (Laboratory for Interdisciplinary CARS Spectroscopy), an ENEA internally funded Project aimed to the realization of an interdepartmental, interdisciplinary CARS facility. TERIN, FSN, and SSPT ENEA Departments, and TERIN-PCU, FSN-TECFIS, and SSPT-TECS Divisions, who financially supported the Project are gratefully acknowledged. MG acknowledges the ICTP grant in the frame of the TRIL Program. Authors kindly thank Dr. M. Tucci (ENEA TERIN-FSN-TEF), for sharing part of the instrumentation used for the Stokes beam characterization.

**References**

[1] Falconieri M., Marrocco M., Merla C., Gagliardi S., Rondino F., Ghezelbash M. "*Characterization of supercontinuum generation in a photonic crystal fiber for uses in multiplex CARS microspectroscopy*" *J. Raman Spectr.* **50**, 1287-1295 (2019)

[2] Gagliardi S., Marrocco M, Rondino F., Palumbo D., Merla C., and Falconieri M. "*Studies of supercontinuum generation in a photonic crystal fiber for use as Stokes beam in a single-laser femtosecond micro-CARS setup*" J. Raman Spectr. **51,** 1934-1941 (2020)

[3] Cheng J. X., X. S. Xie. *Coherent Raman Scattering Microscopy*. Boca Raton, FL USA: CRC Press Taylor & Francis Group, 2013

[4] Kee T.W., M.T. Cicerone. "*Simple approach to one-laser, broadband coherent anti-Stokes Raman scattering microscopy*" Opt. Lett. **29**, 2701-2703 (2004)

[5] Kano H., H.-O Hamaguchi. "*In-vivo multi-nonlinear optical imaging of a living cell using a supercontinuum light source generated from a photonic crystal fiber*" Opt. Express **14**, 2798-2804 (2006)

[6] Andresen E. R., H. N.Paulsen, V. Birkedal, J. Thøgersen, S.R. Keiding. "*Broadband multiplex coherent anti-Stokes Raman scattering microscopy employing photonic-crystal fibers*" J. Opt. So. Am. B **22**, 1934-1938 (2005)

[7] Andresen E. R., C. K. Nielsen, J. Thøgersen, S. R. Keiding. "Fiber laser-based light source for coherent anti-Stokes Raman scattering microspectroscopy." *Opt. Express* **15**, 4848-4856 (2007)

[8] Cheng J.-X., Y. K. Jia, G. Zheng, X. S. Xie. "*Laser-Scanning Coherent Anti-Stokes Raman Scattering Microscopy and Applications to Cell Biology*" Biophys. J. **83**, 502–509 (2002)

[9] Volkmer A., J.-X. Cheng, X. S. Xie. "*Vibrational Imaging with High Sensitivity via Epidetected Coherent Anti-Stokes Raman Scattering Microscopy*" Phys. Rev. Lett. **87**, 023901/1-023901/4 (2001)

[10] Murugkar S., C. Brideau, A. Ridsdale, M. Naji, P. K. Stys, H. Anis. "*Coherent anti-Stokes Raman scattering microscopy using photonic crystal fiber with two closely lying zero dispersion wavelengths*" Opt. Express **15**, 14028-14037 (2007)

[11] Porquez J.G., Slepkov A.D. "*Application of spectral-focusing-CARS microscopy to pharmaceutical sample analysis*." AIP Advances **8**, 095213/1 -7 (2018)

[12] Pegoraro A. F., A. D. Slepkov, A. Ridsdale, J. P. Pezacki, A. Stolow. "*Single laser source for multimodal coherent anti-Stokes Raman scattering microscopy*." Appl. Opt. **49**, F10-F17 (2010)

[13] Pegoraro A.F., A.D. Slepkov, A. Ridsdale, R.K. Lyn, D.J. Moffatt, J.P. Pezacki, B.K. Thomas, L. Fu, L. Dong, M.E. Fermann, A. Stolow. "*High performance multimodal CARS microscopy using a single femtosecond source*" Proc. SPIE *7569*, Multiphoton Microscopy in the Biomedical Sciences X, 756908 (2010)

[14] Porquez J.G., R.A. Cole, J.T. Tabarangao, A.D. Slepkov. "Brighter CARS hypermicroscopy via "spectral surfing" of a Stokes supercontinuum." *Optics Lett.* **42**,: 2255-2258 (2017)

[15] Hilligsøe K.M., T.V. Andersen, H.N. Paulsen, C.K. Nielsen, K. Mølmer, Sø. Keiding, R. Kristiansen, K.P. Hansen, J.J. Larsen. "Supercontinuum generation in a photonic crystal fiber with two zero dispersion wavelengths." *Opt. Express* **12**, 1045-1054 (2004 )

[16] Frosz M.H., P. Falk, O. Bang. "The role of the second zero-dispersion wavelength in generation of supercontinua and bright-bright soliton-pairs across the zero-dispersion wavelength." *Opt. Express* **13**, 6181-6192 (2005)

[17] Newport, App. Notes 29 https://www.newport.com/resourceListing/application-notes *https://www.newport.com* (accessed 09-09-2020).

[18] Corwin, K.L., Newbury, N.R., Dudley, J.M., Coen, S., Diddams, S.A., Weber, K., Windeler, R.S. "*Fundamental noise limitations to supercontinuum generation in microstructure fiber*" Phys. Rev. Lett. **90**, 113904/1-113904/4 (2003)

[19] Newbury, N.R., Washburn, B.R., Corwin, K.L., Windeler, R.S. "*Noise amplification during supercontinuum generation in microstructure fiber*." Opt. Lett. **28**, 944-946 (2003)

[20] Allan, D.W. "*Statistics of Atomic Frequency Standards*" Proceedings of the IEEE,: 221-230 (1966)

[21] Ossenkopf, V. "*The stability of spectroscopic instruments: a unified Allan variance computation scheme*" A&A, **479**, 915-926 (2008)

[22] Lin-Vien D., Colthup N. B., Fateley W. G., Grasselli J.G. "*The Handbook of Infrared and Raman Characteristic Frequencies of Organic Molecules*" Academic Press, London, UK 1991.

[23] Agrawal G. P. "*Nonlinear Fiber Optics*" Academic Press, Oxford, UK 2013.

[24] J. M. Dudley, J. R. Taylor. "*Supercontinuum Generation in Optical Fibers*" Cambridge University Press, Cambridge, UK 2010.

ENEA
Servizio Promozione e Comunicazione
*www.enea.it*

Stampa: Laboratorio Tecnografico ENEA - C.R. Frascati
marzo 2021